Arabian Journal of Geosciences (2021) 14:335
https://doi.org/10.1007/s12517-021-06606-5

ORIGINAL PAPER

Identification of the typical frequency range associated with subsurface gas zones: a study using Hilbert-Huang transform and wavelet analysis

Vaibhav Jayaswal[1,2] · Gaurav Siddharth Gairola[2] · Enamundram Chandrasekhar[1]

Received: 30 July 2020 / Accepted: 23 January 2021

Abstract
Frequency attributes embedded in nonlinear geophysical signals such as well-log data or seismic data can provide vital clues in the effective characterization of the subsurface reservoir. Therefore, it is always important to recognize suitable mathematical techniques that need to be employed to extract such vital information from the nonlinear geophysical data. Several nonlinear mathematical techniques include wavelet analysis, fractal and multifractal analyses, and the fully data-adaptive Hilbert-Huang transform (HHT) technique. In the present study, we employ the HHT and the wavelet analysis techniques to seismic data of the Dutch sector of southern North Sea. We use a small portion of the seismic data, consisting of inline section 133 and time slice section 520 ms of the F3 block, to extract the instantaneous frequency associated with the subsurface gas zone. HHT constitutes two independent techniques, namely, the empirical mode decomposition (EMD) technique and the Hilbert spectral analysis (HSA). While the EMD technique facilitates to decompose the data into different signals of varied frequencies, called intrinsic mode functions (IMFs), the HSA helps to determine the instantaneous amplitudes and frequencies of the IMFs. EMD technique, together with HSA, has delineated a low-frequency spectral signature, believed to be a subsurface gas zone in the chosen data, corroborating the results of earlier studies of the same data sets. The instantaneous frequency range of the gas zone estimated by HSA was validated with the two-dimensional continuous wavelet transform (CWT) of the data sets using a suitable frequency range of Morlet wavelet. Results of the combined HHT and CWT analyses confirmed that the subsurface gas zone could be well identified in the frequency range 14–18 Hz. Results have direct implications *in situ*, in the sense that, by performing CWT analysis of seismic data using a Morlet wavelet in the frequency range 14–18 Hz, one can easily identify the location of subsurface gas zones.

Keywords Hilbert-Huang transform · Subsurface gas zone · Wavelet analysis · Frequency attributes · F3 block Dutch sector North Sea

Introduction

The most comprehensive data sets that are essential for a precise characterization of the hydrocarbon reservoir zones include geophysical well-log data, seismic data, and well-core data, to name a few. Geoscientists unfold the depositional facies of the subsurface reservoir zones, with their physical properties by analyzing such different data sets. A thorough understanding of the behavior of physical properties of the subsurface reservoir zones as a function of depth becomes very important. This is not only possible with advances in exploration technologies for generating the necessary noise-less data but also with the correct use of suitable mathematical techniques to unravel the hidden information from such precious data. For the past several decades, a variety of mathematical techniques, such as the principal component analysis (Wolff and Pelissier-Combescure 1982), the Fourier analysis (Reed et al. 1993), and the semivariogram analysis (Jennings et al. 2000), were widely used for understanding and interpreting the cyclicities present in different geophysical

Responsible Editor: Narasimman Sundararajan

✉ Enamundram Chandrasekhar
esekhar@iitb.ac.in

[1] Department of Earth Sciences, Indian Institute of Technology Bombay, Powai, Mumbai 400076, India

[2] Department of Petroleum Engineering and Earth Sciences, University of Petroleum and Energy Studies, Dehradun 248007, India

Published online: 17 February 2021

well-log data sets. However, the limitations of most of these techniques, including the Fourier transform, are that they are best suited to analyze stationary and linear signals. Since the majority of geophysical signals are nonstationary and nonlinear in nature, identifying the boundaries of subsurface hydrocarbon zones and critical frequencies attributable to them have long been challenging problems for geoscientists. Previous studies have found that the spectral decomposition of seismic data can help in detecting the probable gas zone. However, the conventional signal processing techniques can only tell whether particular frequencies (representative of different formations) of interest are present in the signal or not. They fail to identify which frequencies (formations) occur at what depths. This is known as the space-frequency localization problem, which can be effectively addressed using wavelet analysis (WA) (Mallat 1999; Galiana-Merino et al. 2013; Chandrasekhar and Rao 2012; Hill and Uvarova 2018). Chakraborty and Okaya (1995) employed wavelet analysis on seismic data and discussed the advantages of frequency-time decomposition for its better understanding. Prokoph and Agterberg (2000) used wavelet analysis to determine the high-frequency sedimentary cycles of oil source rocks in well-log data. Frequency attributes provide easy and vital clues on the spatial location of hydrocarbons, while analyzing the relevant geophysical data for their time- or space-frequency localization. Although WA has been quite efficient in time or space-frequency localization in nonlinear data, it relies heavily on the use of a proper mother wavelet, which often is not easy to identify. In such situations, the use of an alternate approach, which is a fully data-adaptive and yet best suited to analyze the nonlinear geophysical data, will be more worthwhile and appropriate to implement and extract the required information from the signals. Subhakar and Chandrasekhar (2016) employed the data-adaptive multifractal analysis to different well-log data sets of the western off-shore basin of India and distinguished different wells based on their shale content. They also have confirmed that the presence of long-range correlations in well-log data led to their multifractal behavior. Another fully data-adaptive technique, which can effectively help in analyzing the nonlinear signals, is the Hilbert-Huang transform (HHT) developed by Huang et al. (1998) and Huang and Wu (2008). HHT consists of two independent techniques, such as the empirical mode decomposition (EMD) technique and the Hilbert spectral analysis (HSA) (Huang et al. 1998). While the EMD technique decomposes the signal into oscillatory signals of different frequencies called intrinsic mode functions (IMFs) through a sifting process, the HSA can be used to determine the instantaneous frequencies and amplitudes of each IMF. Therefore, the HHT technique holds an advantage over other spectral decomposition methods in unravelling the space-frequency characteristics of the signal. Gairola and Chandrasekhar (2017) employed the HHT technique jointly with heterogeneity analysis on the same data sets used by Subhakar and Chandrasekhar (2016) and distinguished different wells in the study area based on the estimated degree of lateral heterogeneity in the thick limestone reservoir zone. Schroot et al. (2005) identified a subsurface gas zone by analyzing seabed sediment samples collected from the southern North Sea zone. Later, Hashemi et al. (2008) used limited seismic data sets from the same zone and supported the findings of Schroot et al. (2005), albeit with a poor resolution of the identified subsurface gas zone. In the present study, we apply the HHT technique to the seismic sections of inline 133 and time slice 520 ms of the F3 block "in the Dutch sector of southern North Sea" to determine the instantaneous frequency range associated with the gas zone evident in both the seismic sections. We next validate the estimated instantaneous frequency range attributable to the gas zones, by applying a continuous wavelet transform to both the seismic sections using Morlet wavelet of different frequencies.

Geology of the study area

Figure 1 shows the location (N 54° 52′ 0.86″/E 4° 48′ 47.07″) of the F3 block in the Dutch sector of the southern North Sea basin, whose seismic data was used in the present study. The stratigraphy of the North Sea basin is described in three different geological eras Paleozoic, Mesozoic, and Cenozoic. During the Cenozoic era, this region was characterized by a thermally subsiding epicontinental basin, most of which was confined by landmass (Sørensen et al. 1997). The North Sea group refers to the rock formation of the North Sea, which was formed during the Paleogene and Neogene (in the Cenozoic era) and is further divided into three sub-formations: the Lower, the Middle, and the Upper North Sea divisions (Ishak et al. 2018). While the Lower and Middle divisions correspond to the Paleogene period, the Upper division corresponds to the Neogene period (Ishak et al. 2018). The Lower North Sea group was deposited under several marine sedimentation cycles, which consist of grey sands, sandstones, and clay. This sub-group is bounded by the overlying deposits of the Middle North Sea formation and an unconformity at the bottom. The Middle North Sea formation was deposited in a marine environment along with some lagoon and coastal marine sediments which consists of sand, silt, and clay with the dominant sand distribution towards the southern margin of the basin. The Upper North Sea formation was deposited in a shallow marine environment with an influx of fluvial and lacustrine origin which consists of clay and fine- to coarse-grained sands along with gravel, peat, and brown coal seams (Van Adrichem Boogaert and Kouwe 1993; Rondeel et al. 1996). Towards the north and west part of the basin, coarse- to fine-grained sand trend is observed. This sub-group is bounded by the seafloor as the upper boundary and Middle

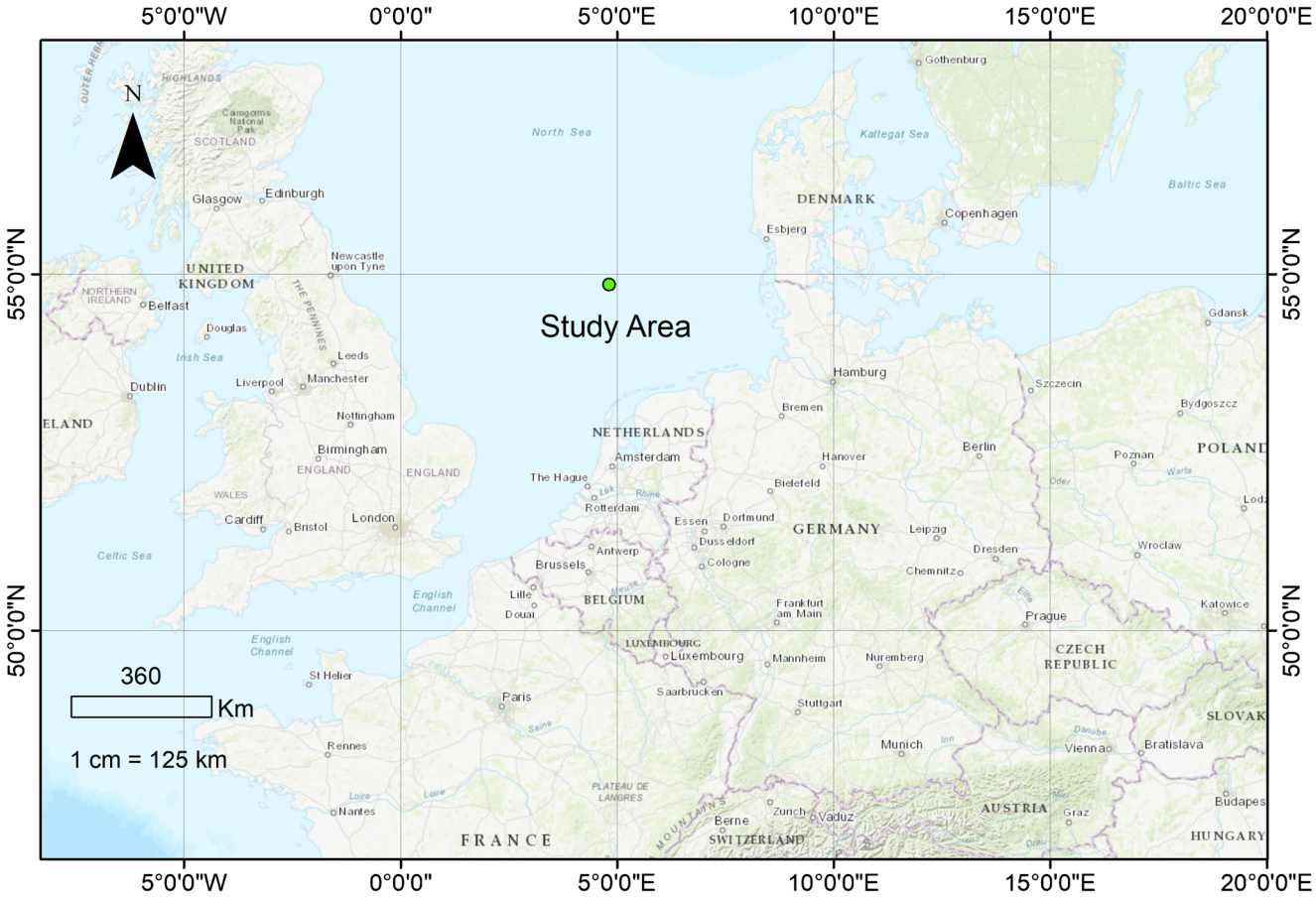

Fig. 1 Geographical location (N 54° 52′ 0.86″/E 4° 48′ 47.07″) of the F3 block in the Dutch sector of the southern North Sea

North Sea group as the lower boundary. The deltaic system started during the Oligocene period. The uplift in the late Miocene causes huge sedimentation influx in the North Sea region of the Dutch sector. The increased sediment load causes the underlying salt to move. As a result, several unconformities are formed during the Pliocene. The oil and gas traps in the North Sea are the results of the extensional tectonics due to failed rifting. The present study focuses on the biogenic gas deposit of Neogene age in the Upper North Sea formation.

Data

3D seismic data of the F3 block corresponding to the Upper Cenozoic fluviodeltaic system in the Dutch sector of southern North Sea was used in the present study. The data volume contains inline range from 100 to 750, crossline range from 300 to 1250, and time slices from 0 to 1848 ms, sampled at a rate of 4 ms. The data used in this study is freely available and can be downloaded from https://terranubis.com/datainfo/Netherlands-Offshore-F3-Block-Complete. The available data has already been subjected to a structurally oriented dip-steered median filtering (see Jaglan et al. 2015) with a radius of two traces to remove the random noise and augment the laterally continuous seismic events. The iterative dip-steered median filter attenuates the random noise better than F-k least squares filter due to edge preserving characteristics (see Huo et al. 2017). Hashemi et al. (2008) used only the inline section 133 data and applied the multilayer perceptron (MP) and support vector (SV) classifiers to identify the presence of gas zone in the study area. However, because of the use of such limited data, the resolution of the delineated subsurface gas zone was very poor. This has prompted us to use the additional time slice data of 520 ms together with the inline section 133 data, to assess the areal extent of the anomalous gas zone. Therefore, for the present study, we have used a cropped seismic volume, consisting of inline range from 100 to 600, crossline range from 300 to 1250, and time from 0 to 1848 ms.

Methodology

Empirical mode decomposition technique

EMD technique facilitates to systematically extract different frequency components of the signal under investigation in an

iterative fashion till the signal becomes monotonic when further extraction of frequencies will not be possible. The monotonic frequency component is called the residue, which represents the lowest frequency component of the signal and thus signifies the overall trend present in the signal. The step-wise description of the EMD algorithm is as follows:

1. Make the upper envelope (E_{max}) and the lower envelope (E_{min}) of the input signal, $s(t)$, using its local maxima and minima respectively by cubic spline interpolation and compute the mean, m_1 of both the envelopes.
2. Compute the first proto IMF, x_1, by removing m_1 from original signal,

$$x_1 = s(t) - m_1. \tag{1}$$

3. If x_1 still contains maxima and minima, steps 1 and 2 should be repeated to get

$$x_{11} = x_1 - m_{11}. \tag{2}$$

Accordingly, after k iterations, we shall have,

$$x_{1k} = x_{1(k-1)} - m_{1k}. \tag{3}$$

The stopping criterion for this repeated operation is defined, based on the following: (a) the number of maxima and number of zero crossings must be equal or differ at most by one and, (b) m_1 should be zero for the entire signal (Huang et al. 1998). While the condition (a) ensures that the signal under investigation should be devoid of any local fluctuations within it, the condition (b) ensures that the Hilbert transform determines extraction of correct instantaneous frequencies in the data. Mathematically, the stopping criterion is defined as the normalized squared difference between two successive sifting operations, defined as

$$SD_k = \frac{\sum_{i=0}^{N} [x_{k-1}(i) - x_k(i)]^2}{\sum_{i=0}^{N} [x_{k-1}^2(i)]} \tag{4}$$

where N is the total number of data points.

4. Preferably, choose SD_k as small as possible, say $SD_k \leq 0.1$, as the stopping criterion to determine each IMF after k iterations. That means, once the defined stopping criterion is satisfied after the first set of k iterations, then we get the first IMF, denoted as IMF_1, which signifies the highest frequency present in the data. The condition $SD_k \leq 0.1$ is rather arbitrary and largely depends on the data quality. Higher limiting values for SD_k are generally set for poor-quality data and vice-versa for better estimates of IMFs (Gairola and Chandrasekhar 2017).
5. To determine the second IMF (IMF_2), calculate the residue, r_1 by subtracting IMF_1 from the original signal $s(t)$ and treat r_1 as a new signal and repeat steps 1–4. IMF_2 will be of lower frequency than IMF_1.
6. Repeat steps 1–5 for each data trace to get all the IMFs associated with it. Figure 2 depicts the above procedure in the form of a simple flowchart. One can get back the original signal, by synthesizing all the IMFs together with the monotonic residue, r_n, using the formula,

$$s(t) = \sum_{i=1}^{n} IMF_i - r_n \tag{5}$$

The above procedure was applied to each trace of the inline section 133 and time slice 520 ms. A set of five IMFs corresponding to each trace of inline section 133 and another set of five IMFs corresponding to each trace of time slice 520 ms were obtained. IMF_1 of all the traces of inline section 133 are combined to form IMF_1 section of inline section 133. Similarly, IMF_1 of all the traces of time slice 520 ms are combined to form IMF_1 section of time slice 520 ms. Likewise, the rest of the IMF sections corresponding to IMF_2 to IMF_5 are also obtained. Figures 3 and 4 depict the IMF sections corresponding to inline section 133 and time slice 520 ms respectively.

Hilbert spectral analysis

Hilbert spectral analysis (HSA) was applied each IMF section, to compute its corresponding instantaneous amplitude and instantaneous frequency. The Hilbert transform facilitates to obtain the analytic representation $A(t)$ of a signal $s(t)$ under study, which is defined as

$$A(t) = s(t) + i\hat{s}(t) \tag{6}$$

where $\hat{s}(t)$ defines the Hilbert transform of $s(t)$. The instantaneous amplitude, $a(t)$, the instantaneous phase, $\theta(t)$, and the instantaneous frequency, $\omega(t)$, are defined as

$$a(t) = \left(s(t)^2 + \hat{s}(t)^2\right)^{1/2} \tag{7}$$

$$\theta(t) = \tan^{-1}\left(\frac{\hat{s}(t)}{s(t)}\right) \tag{8}$$

$$\omega(t) = \frac{d(\theta(t))}{dt} \tag{9}$$

The results of HSA performed on all the IMFs of inline section 133 and time slice 520 ms are shown in Figs. 5 and 6 respectively. The instantaneous frequencies, $\omega(t)$,estimated for each IMF corresponding to inline section 133 and time slice section 520 ms are listed in Table 1.

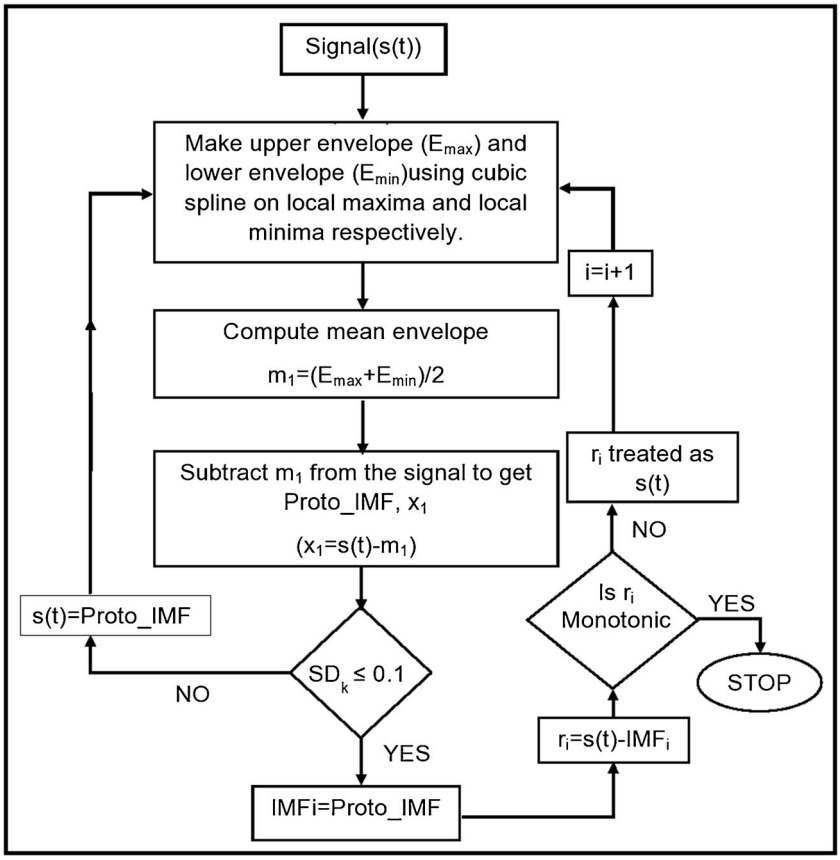

Fig. 2 Flowchart representing the algorithm of EMD technique

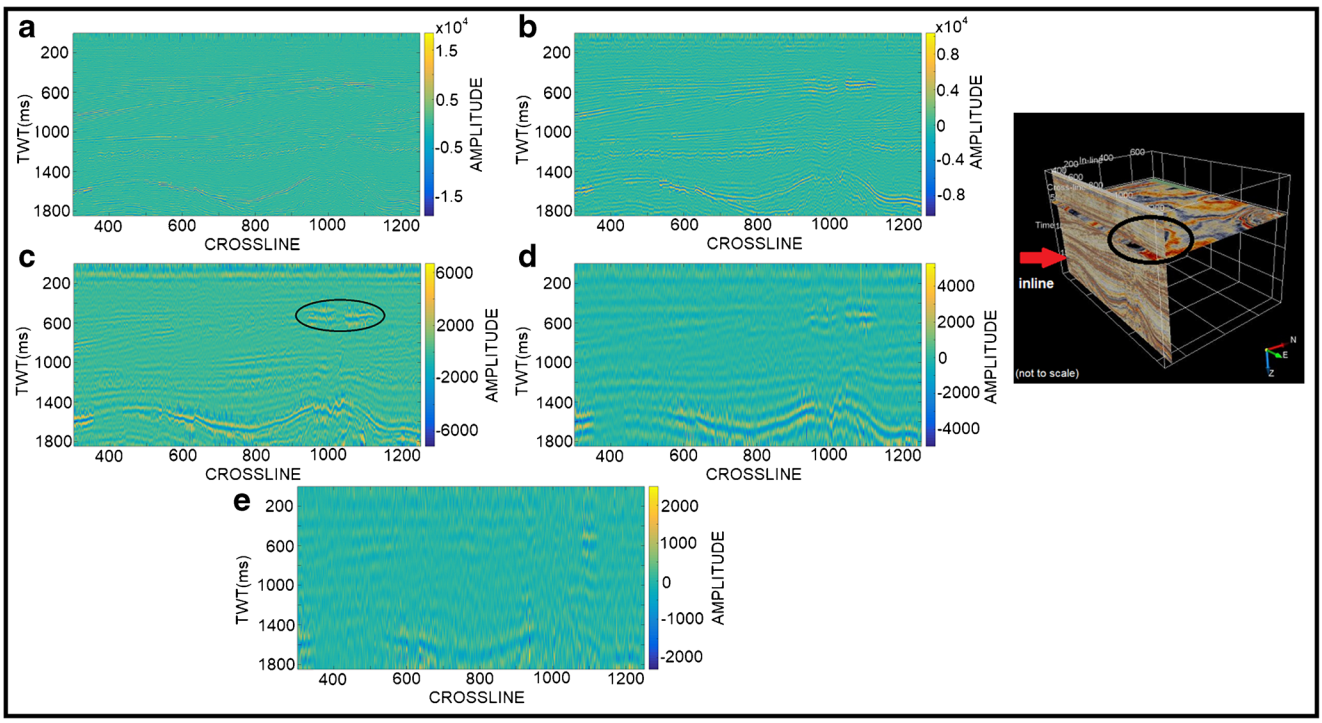

Fig. 3 Intrinsic mode functions (IMFs) of inline section 133 corresponding to **a** IMF_1, **b** IMF_2, **c** IMF_3, **d** IMF_4, **e** IMF_5. Inset shows the 3D representation of inline and time slice sections of the seismic data volume

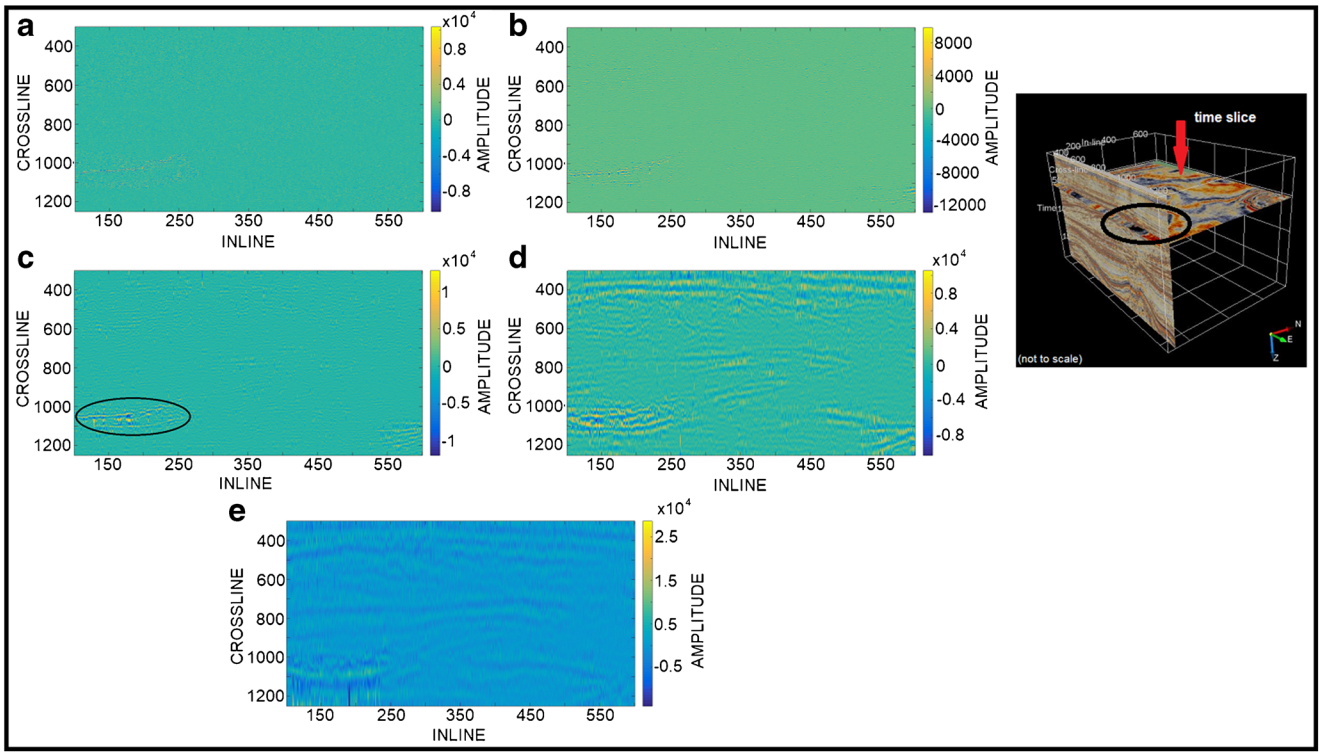

Fig. 4 Same as Fig. 3, but for time slice 520 ms

Continuous wavelet transformation

Continuous wavelet transformation (CWT) can be defined as the inner product of the mother wavelet or analyzing wavelet, $\psi(t)$, and the signal, $f(t)$, given by

$$CWT\ (\tau, s) = \frac{1}{\sqrt{s}} \int_{-\infty}^{\infty} f(x)\psi\left(\frac{t-\tau}{s}\right) dt \tag{10}$$

where $s > 0$ indicates the scale and τ indicates the translation parameter. s is analogous to frequency, in the sense that higher scales (low frequencies) provide details of long-wavelength features of the signal and lower scales (high frequencies) provide details of the short-wavelength features of the signal. τ refers to time information in the transformed domain. The above equation explains that the wavelet transformation gives a measure of the similarity between the signal and the wavelet function. Such a measure at any particular s and τ is identified by a wavelet coefficient. The larger the value of this coefficient, the higher the similarity between the signal and the wavelet at τ and s and vice-versa. More details about the CWT operation can be found in Daubechies (1992), Mallat (1999), Chandrasekhar and Rao (2012), and references therein. In the present study, we have used Morlet wavelet which is defined as the product of a complex exponential wave and a Gaussian envelope. Mathematically, it is expressed as

$$\psi(t) = \pi^{-1/4} e^{i\omega t} e^{-t^2/2} \tag{11}$$

The shape of real part of the above function, which is used in the present analysis, is shown in Fig. 7. In the present study, we have implemented CWT analysis on the inline section 133 (Fig. 8) and time slice 520 ms (Fig. 9) using the Morlet wavelet, only to validate frequency attributes of the gas zone, determines by the HHT.

Table 1 The instantaneous frequencies estimated for each IMF corresponding to inline section 133 and time slice section 520 ms. The frequencies emphasized in bold font against IMF_3 signify the identified frequency range for subsurface gas zone, which is also confirmed by continuous wavelet transformation

IMF number	Frequency (Hz)	
	Inline section 133	Time slice 520 ms
IMF_1	53.8	67.8
IMF_2	28.4	37.4
IMF_3	**14.5**	**17.4**
IMF_4	7.5	7.4
IMF_5	4.12	3.3

Results and discussion

A careful observation of Fig. 3 reveals that between the crosslines 950–1020 and 1050–1150 and the two-way travel time from 400–600 ms corresponding to IMF_3 section (Fig.

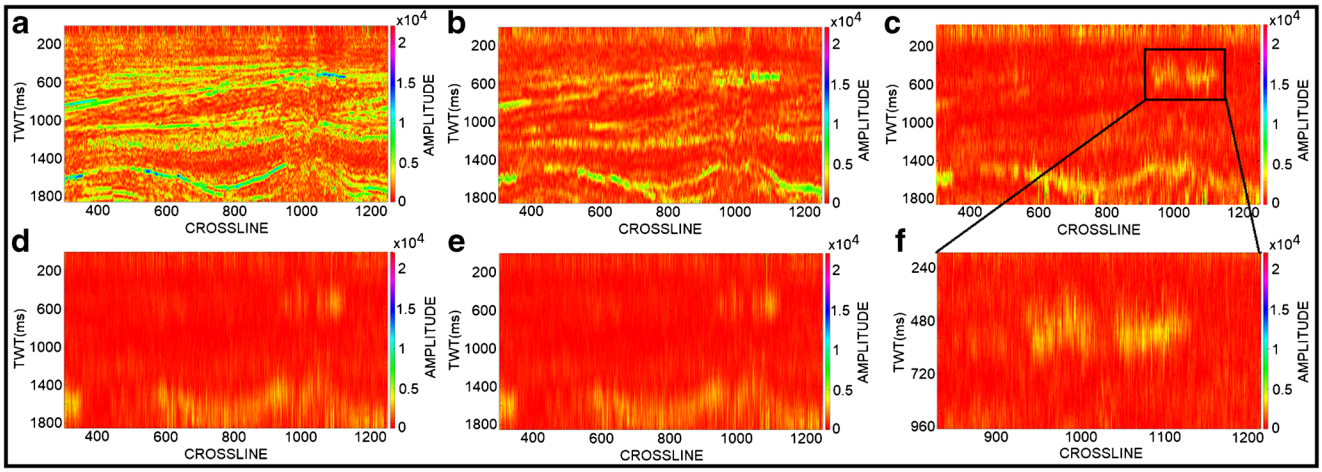

Fig. 5 Illustration of instantaneous frequencies obtained after applying Hilbert spectral analysis (HSA) corresponding to **a** IMF_1, **b** IMF_2, **c** IMF_3, **d** IMF_4, **e** IMF_5 of inline section 133, **f** zoomed portion of the gas zone anomaly seen in (**c**)

3c), a prominent and well-resolved anomalous gas zone (circled) could be clearly identified, compared to the features at the same area in other IMF sections (Fig. 3a, b, d, e). Similarly, the corresponding zone in time slice of 520 ms is also clearly seen, having high resolution (Fig. 4c), compared to other IMFs in the same times slice section (Fig. 4a, b, d, e). Among the other IMFs and Hilbert spectra of inline section 133 (Figs. 3 and 5) and time slice 520 ms sections (Figs. 4 and 6), the IMF_1 (Figs. 3a, 4a, 5a, 6a) and IMF_2 (Figs. 3b, 4b, 5b, 6b), representatives of high frequencies in the data appear to have interspersed with the frequencies of other adjoining lithology and thus the suspected anomalous gas zone could not be clearly delineated. Similarly, the IMF_4 (Figs. 3d and 5d; Figs. 4d and 6d) and IMF_5 (Figs. 3e and 5e; Figs. 4e and 6e), representatives of low frequencies in the data, show smeared resolution and thus could not clearly delineate the gas zone. However, the resolution of the anomalous gas zone seen in IMF_3 (Figs. 3c and 4c) and in the corresponding Hilbert spectra of inline section 133 (Fig. 5c, f) and time slice section 520 ms (Fig. 6c, f) is very high.

A comparison of the estimated instantaneous frequencies of IMFs corresponding to inline section 133 and time slice section 520 ms (Table 1) and their respective Hilbert spectra (Figs. 5 and 6) clearly shows that the presence of gas zone is clearly seen with a high resolution in the frequency range of 14.5–17.4 Hz (Table 1) corresponding to the spectra of IMF_3 of inline section 133 (Fig. 5c, f) and time slice 520 ms (Fig. 6c, f). Castagna et al. (2003) explained that such low-frequency attributes in the seismic data indicate the presence of subsurface gas zones. Castagna et al. (2003) also showed that the resolution of subsurface gas zone is very poor at frequencies less than 12 Hz. Corroborating their observations, our results also clearly show that at the instantaneous frequencies corresponding to IMF_4 and IMF_5 of inline section 133 (Fig. 5d, e) and time slice of 520 ms (Fig. 6d, e), which are less than 14.5 Hz (see Table 1), the resolution of the anomalous gas zone is very poor. Since the resolution of the anomalous gas zone is very high at the instantaneous frequency of 14.5 Hz corresponding to IMF_3 of inline section 133 and

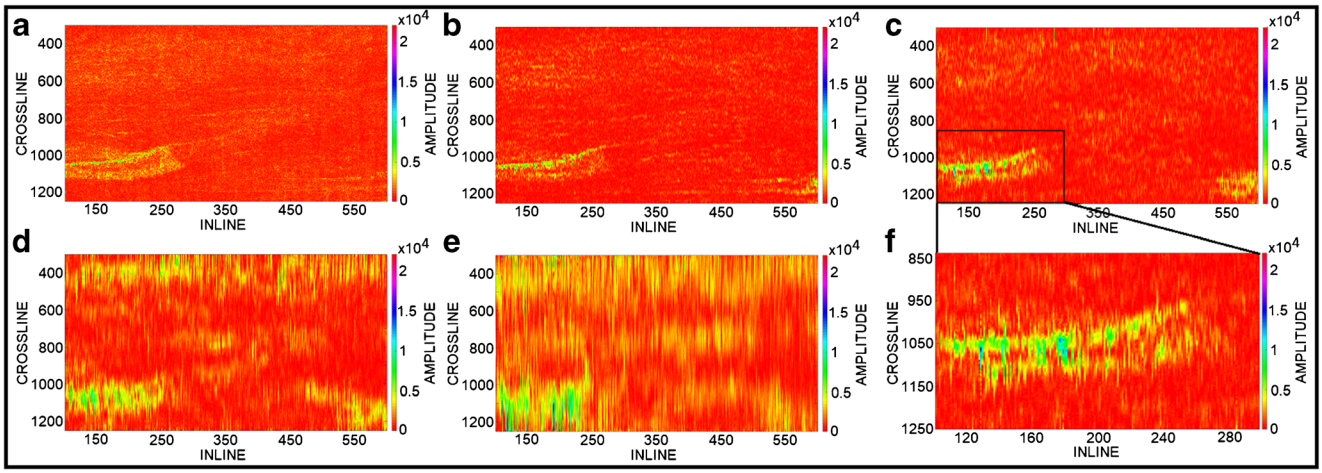

Fig. 6 Same as Fig. 5, but for time slice of 520 ms

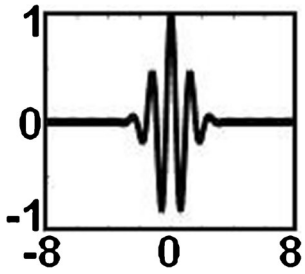

Fig. 7 Illustration of real part of Morlet wavelet

at 17.4 Hz corresponding to IMF_3 of time slice of 520 ms (see Table 1), we believe the optimum frequency range associated with subsurface gas zone could be 14–18 Hz. While Castagna et al. (2003) advocated that the subsurface gas zones are poorly resolved at frequencies less than 12 Hz, we extend their observation and further argue that the subsurface gas zones are also poorly resolved at frequencies greater than 18 Hz. Thus, the systematic decomposition of the data based on their frequency content, in the form of IMFs through EMD technique and estimating their respective instantaneous frequencies by HSA, has been found to be very effective in clearly attributing the correct frequency range associated with gas zones in seismic data and thus our results show that the optimal frequency range attributable to subsurface gas zones is 14–18 Hz.

To further validate our above observation, we have performed continuous wavelet transform (CWT) on the inline section 133 and time slice 520 ms using Morlet wavelet of four different scales, having corresponding frequencies: 5 Hz, 15 Hz, 30 Hz, and 45 Hz. Figures 8 and 9 depict the wavelet scalograms representing the space-frequency localization of anomalous subsurface gas zones corresponding to inline section 133 and time slice 520 ms respectively. In agreement with the results obtained for inline section 133 by EMD analysis (Figs. 3 and 4) and for time slice 520 ms by Hilbert spectral analysis (Figs. 5 and 6), their corresponding wavelet scalograms corresponding to 5 Hz, (Figs. 8a and 9a), 30 Hz (Figs. 8c and 9c), and 45 Hz (Figs. 8d and 9d) also clearly show a poor resolution of the identified anomalous subsurface gas zones. However, the wavelet scalograms corresponding to 15 Hz (Figs. 8b and 9b) clearly show that the CWT analysis of inline section 133 and time slice 520 ms data with Morlet wavelet show highest resolution for the subsurface gas zone. Particularly, the twin gas zones located adjacent to each other as seen in the Hilbert spectra of inline section 133 (see Fig. 5c and f) and time slice section of 520 ms (Fig. 6c and f) are clearly delineated in their respective CWT results shown in Fig. 8b and Fig. 9b.

These observations unequivocally confirm the very good agreement between the instantaneous frequency range of 14–18 Hz determined by HHT (Table 1) and the CWT analysis carried out with Morlet wavelet at 15 Hz, suggesting the optimum frequency range that is best suitable to identify the subsurface gas zone is 14–18 Hz.

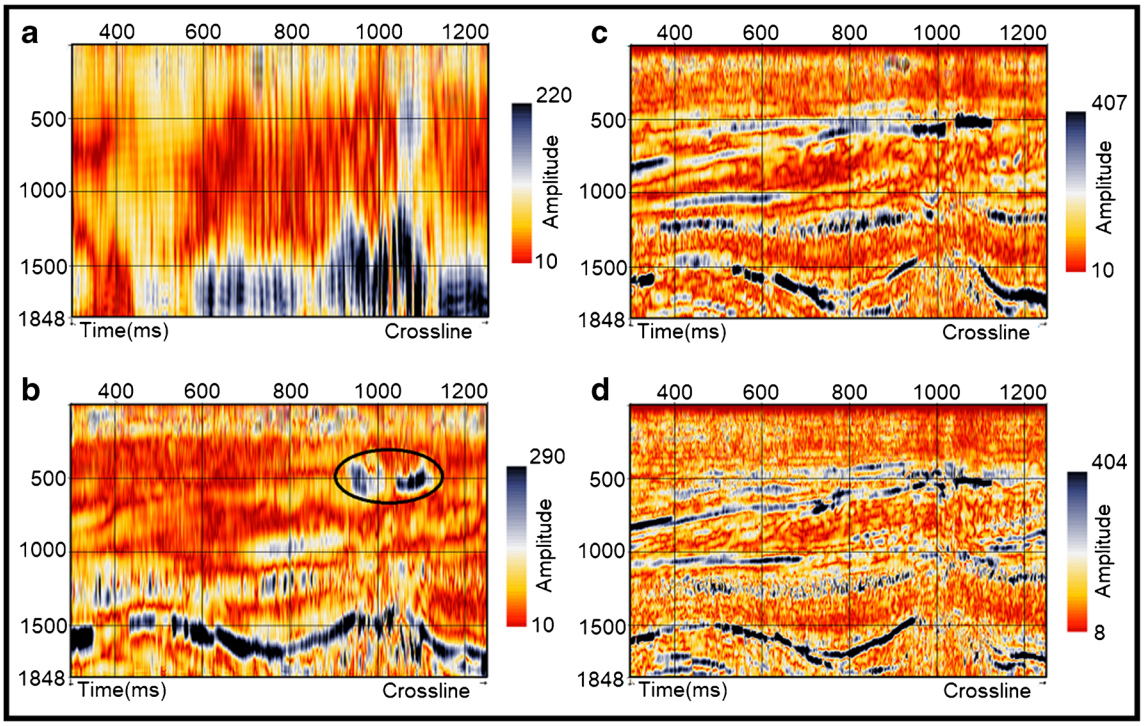

Fig. 8 Illustration of continuous wavelet transform of inline section 133 using Morlet wavelet of four different scales having corresponding frequencies: **a** 5 Hz, **b** 15 Hz, **c** 30 Hz, and **d** 45 Hz

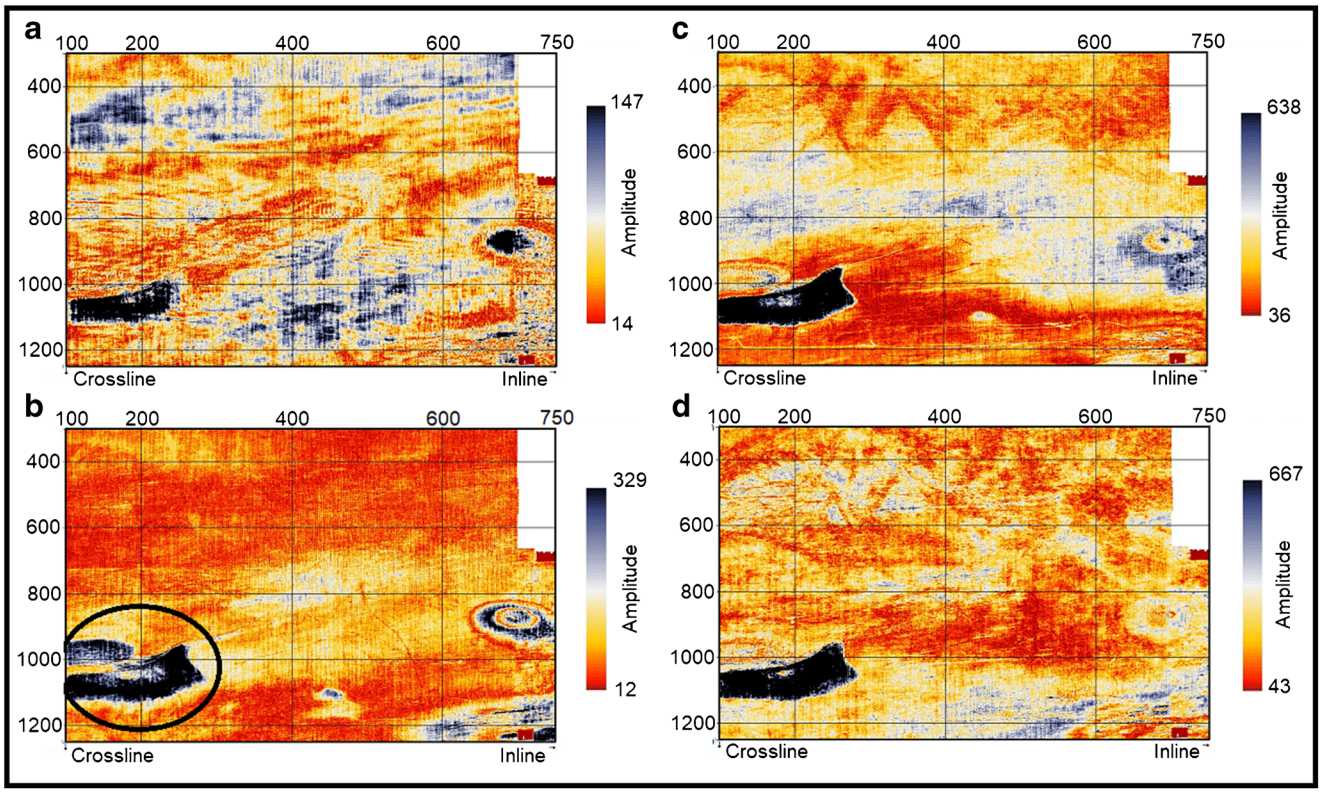

Fig. 9 Same as Fig. 8, but for time slice of 520 ms

Conclusions

The fully data-adaptive and nonlinear HHT technique proved its worthiness in identifying the frequency characteristics associated with the subsurface gas zone. While the EMD technique has effectively helped to delineate the anomalous subsurface gas zone with high resolution in IMF_3 of the selected seismic data, the HSA facilitated to estimate the instantaneous frequency range associated with IMF_3 as 14–18 Hz. Through this study, we extend the observations made by Castagna et al. (2003) and argue that subsurface gas zones show poor resolution not only at frequencies less than 12 Hz but also at frequencies greater than 18Hz. CWT analysis carried out using Morlet wavelet of 15Hz frequency further validates this observation. Through this study, we have identified a typical frequency range of 14-18 Hz attributable to the subsurface gas zones as demonstrated and validated by HHT and CWT analyses of 3D seismic data. The scientific importance of our study highlights the fact that by simply performing the CWT analysis of seismic data using the Morlet wavelet in the frequency range 14–18 Hz, one can easily identify the subsurface gas zones. Through our above study, we advocate that HHT and CWT techniques as efficient investigating tools to quickly scan the seismic data for the frequency attributes and their space/time localization, to help identify the location of potential subsurface gas zones.

Acknowledgements The authors thank all those who have recorded the high-quality 3D seismic data of the F3 block of Dutch sector of southern North Sea. VJ thanks the International Association for Mathematical Geosciences (IAMG) for providing him the travel grants to present part of the results of the present study at the 20th Annual conference of the IAMG, held in August 2019 at State College, PA, USA. VJ also thanks IIT Bombay for providing him the postgraduate fellowship. The authors express their sincere thanks to the two anonymous referees and the handling editor for their meticulous and critical comments, which have significantly improved the quality of the paper.

Compliance with ethical standards

Conflict of interest The authors declare that they have no competing interests.

References

Castagna JP, Sun S, Siegfried RW (2003) Instantaneous spectral analysis: detection of low-frequency shadows associated with hydrocarbons. Lead Edge 22:120–127

Chakraborty A, Okaya D (1995) Frequency-time decomposition of seismic data using wavelet-based methods. Geophysics 60:1906–1916

Chandrasekhar E, Rao VE (2012) Wavelet analysis of geophysical well-log data of Bombay Offshore Basin, India. Math Geosci 44(8):901–928. https://doi.org/10.1007/s11004-012-9423-4

Daubechies I (1992) Ten lectures on wavelets. Society for Industrial and Applied Mathematics, Philadelphia

Gairola GS, Chandrasekhar E (2017) Heterogeneity analysis of geophysical well-log data using Hilbert Huang transform. Physica A 478: 131–142. https://doi.org/10.1016/j.physa.2017.02.029

Galiana-Merino JJ, Rosa-Herranz JL, Rosa-Cintas S, Martinez-Espla JJ (2013) Seismic wave tool: continuous and discrete wavelet analysis and filtering for multichannel seismic data. Comput Phys Commun 184:162–171

Hashemi H, Tax DMJ, Duin RPW, Javaherian A, de Groot P (2008) Gas chimney detection based on improving the performance of combined multilayer perceptron and support vector classifier. Nonlinear Process Geophys 15:863–871

Hill EJ, Uvarova Y (2018) Identifying the nature of lithogeochemical boundaries in drill holes. J Geochem Explor 184:167–178

Huang NE, Wu Z (2008) A review on Hilbert-Huang transform: method and its application to geophysical studies. Rev Geophys 46(2): RG2006. https://doi.org/10.1029/2007RG000228

Huang NE, Shen Z, Long SR, Wu MC, Shih HH, Zheng Q, Yen NC, Tung CC, Liu HH (1998) The empirical mode decomposition and the Hilbert spectrum for nonlinear and nonstationary time series analysis. Proc R Soc Lond Ser A Math Phys Eng Sci 454:903–993

Huo S, Zhu W, Shi T (2017) Iterative dip-steering median filter. J Appl Geophys 144:151–156

Ishak MA, Islam MA, Shalaby MD, Hasan N (2018) The application of seismic attributes and wheeler transformations for the geomorphological interpretation of stratigraphic surfaces: a case study of the F3 Block, Dutch Offshore Sector, North Sea. Geosciences 8

Jaglan H, Qayyum F, Huck H (2015) Unconventional seismic attributes for fracture characterization. First Break 33:101–109

Jennings JW, Ruppel SC, Ward WB (2000) Geostatistical analysis of permeability data and modeling of fluid-flow effects in carbonate outcrops. SPE Reserv Eval Eng 3:292–303

Mallat S (1999) A wavelet tour of signal processing, 2nd edn. Academic Press, San Diego, 620 p

Prokoph A, Agterberg FP (2000) Wavelet analysis of well-logging data from oil source rock, Egret Member, Offshore Eastern Canada. AAPG Bull 84:1617–1632

Reed MJ, Nguyen HV, Chambers RE (1993) Computing the Fourier transform in geophysics with the transform decomposition DFT. Geophysics 58(11):1707–1709

Rondeel HE, Batjes DAJ, Nieuwenhuijs WH (eds) (1996) Geology of gas and oil under the Netherlands, 1st edn. Kluwer Academic Publishers, 284 p

Schroot BM, Klaver GT, Schuttenhelm RGT (2005) Surface and subsurface expression of gas seepage to the seabed-examples from southern North Sea. Mar Pet Geol 22:499–515

Sørensen JC, Gregersen U, Breiner M, Michelsen O (1997) High frequency sequence stratigraphy of upper Cenozoic deposits. Mar Pet Geol 14:99–123

Subhakar D, Chandrasekhar E (2016) Reservoir characterization using multifractal fluctuation analysis of geophysical well-log data. Physica A 445:57–65. https://doi.org/10.1016/j.physa.2015.10.103

Van Adrichem Boogaert HA, Kouwe WFP (1993) Stratigraphic nomenclature of the Netherlands, revision and update by RGD and NOGEPA. Mededelingen Rijks Geologische Dienst 50:1–40

Wolff M, Pelissier-Combescure J (1982) FACIOLOG: automatic electrofacies determination. Society of Petrophysicists and Well-Log Analysts, annual logging symposium, 6–9, paper FF